

# Geometrically Thin Disk Accreting Into a Black Hole

N. Afshordi & B. Paczyński

Princeton University Observatory, Princeton, NJ 08544–1001, USA

E-mail: afshordi@astro.princeton.edu

E-mail: bp@astro.princeton.edu

## ABSTRACT

A numerical model of a steady state, thin and isothermal accretion disk is presented. We demonstrate that ‘zero torque’ inner boundary condition is a reasonable approximation provided that the disk thickness, including the thickness of the torquing magnetic fields, is small. It is likely that this conclusion is correct also for non-isothermal and non-steady disks, as long as the total thickness at the inner edge,  $H_{in}$ , is much smaller than the radius there,  $r_{in} \approx r_{ms}$ . The very existence of thin disks is not proven or disproven in this work, but such disks are believed to exist for moderate accretion rates.

*Subject headings:* black hole physics — accretion disks — magnetic fields

## 1. Introduction

A Newtonian theory of geometrically thin accretion disks was developed in classical papers by Pringle & Rees (1972), Shakura & Sunyaev (1973) and Lynden-Bell & Pringle (1974), generalized for a relativistic case by Novikov & Thorne (1973), and reviewed by Pringle (1981). A relativistic effect: the bending of light trajectories leading to direct illumination of the disk by itself, was first elaborated and calculated by Cunningham (1975, 1976). This is marginally important for a disk accreting onto a Schwarzschild black hole, but it is very important for the Kerr case, introducing large non-local effects to the mass, momentum and energy balance. In these early papers a geometrically thin disk accreting onto a black hole had the inner boundary at the marginally stable orbit,  $r_{ms}$ , and the gas was freely falling on a tight spiral inwards of  $r_{ms}$ .

There was some confusion about the nature of gas flow near the inner disk edge (Stoeger 1976). The issue was first understood as a transition from subsonic accretion to supersonic accretion for geometrically thick disks (Abramowicz et al. 1978), and later for geometrically thin disks (Muchotrzeb & Paczyński 1982). These papers, and many

more, were reviewed by Abramowicz & Kato (1989), who presented a general discussion of the transonic flows in accretion disks. In particular, they pointed out that while such a transition is necessary for the existence of a steady state accretion, it does not guarantee that a sensible global solution exists (cf. their Fig. 2).

All the papers written in 1970s and 1980s adopted some form of ‘alpha’ viscosity, as there was no quantitative physical model for the effective transport of angular momentum and the dissipation of energy within accretion disks. Perhaps the best qualitative description of these processes was given by Galeyev et al. (1979). A major breakthrough was made by Balbus & Hawley (1991) and Hawley & Balbus (1991), who rediscovered a powerful magneto-rotational instability in weakly magnetized disks, and pointed out its relevance to accretion. A flood of papers followed, with powerful computers making it possible to model time dependent accretion flows in 2-D (Armitage 1998, Stone et al. 1999, Agol et al. 2001, Stone & Pringle. 2001) and in 3-D (Flemming et al. 2000, Hawley et al. 2001, Armitage 2001a,b, Armitage et al. 2001, Reynolds & Armitage 2001, Reynolds et al. 2001, Sano & Inutsuka 2001).

A lot of semi-analytical and numerical work was done for the ADAF and CDAF models (cf. Ball, Narayan & Quataert 2001, and references therein). It appears that at very high and at very low accretion rates disks are geometrically thick, while thin disks may exist only for moderate accretion rates. If this view is correct then the early work on geometrically thin accretion disks may be relevant for  $0.01 < L/L_{Edd} < 0.1$ .

Yet another way to modify the picture was proposed by Blandford and Znajek (1977), who pointed out that a large scale magnetic field may thread a black hole, and it may extract its rotational energy. In recent years the original picture was modified, making it more likely that the energy extracted from a spinning black hole is transferred to the inner parts of the disk, rather than directly to a distant load (Livio, Oglive & Pringle 1999, Agol & Krolik 2000, Li 2000a,b). Recent XMM observations of an AGN named MCG-6-30-15 were claimed to support this possibility XMM (Wilms et al. 2001). If the interpretation of the data is correct, then the traditional no torque inner boundary condition (cf. Abramowicz & Kato 1989, and references therein) may not apply even to thin disk. This would appear to confirm a theoretical claim by Krolik (1999), Gammie (1999), and Agol & Krolik (2000) that the no torque inner boundary condition is not justified.

One of us (BP) argued that no torque inner boundary condition is natural if the accretion disk is geometrically thin (Paczynski 2000), but the referee could not be convinced. Apparently, the arguments while simple were not complete. The purpose of this paper is to outline the simple reasoning behind thin disk models of 1970s and 1980s, to present the arguments for the no torque inner boundary condition, and the assumptions involved.

In Sec. 2, we derive the equations that describe a thin and steady state isothermal accretion disk while in Sec. 3, solutions of these equations and their topologies are studied numerically. Sec. 4, describes an analytical method to identify solutions of different nature. Sec. 5 discusses some of the physical results of our work and, finally, Sec.6 concludes this paper.

## 2. A Thin Disk

The modern 2-D and 3-D numerical simulations provided the first quantitative and meaningful insight into the actual physics of accretion disk, and as computer power increases and the codes become more sophisticated a steady progress is to be expected. However, at this time there are significant limitations. The accretion flows are relatively thick, the outer boundary is not very far out, the cooling processes are not included, the time integrations can be carried out for a rather modest multiple of the dynamical time scale. The current ADAF or CDAF or variants of Blandford - Znajek models do not exceed a toy model level. This is both, natural and useful, and the quantitative understanding will be improved with time. For the same reason it is useful to have a good quantitative understanding of semi-analytical models of geometrically thin accretion disks. The simple toy models will remain useful even when the 3-D numerical approach will provide full quantitative comparison with the future observations.

The argument presented by Paczyński (2000) in favor of applicability of a no torque inner boundary condition was very simple. Geometrically thin, steady state disk accretion onto a black hole was subsonic at  $r > r_{in}$ , and supersonic at  $r < r_{in}$ , with the inner disk radius  $r_{in}$  located near the marginally stable orbit, at  $r_{ms}$ . The specific angular momentum at  $r_{in}$  is  $l_{in}$ , and it satisfies the equation

$$\frac{l_{in} - l_0}{l_{in}} \approx \alpha \frac{H_{in}}{r_{in}} \ll 1, \quad (1)$$

(cf. eq. 4 in Paczyński 2000), where  $l_0 \approx l_{ms}$  is the angular momentum integration constant,  $H$  is the disk thickness, and  $\alpha$  is the viscosity parameter. Current 3-D numerical calculations for thick disks and tori indicate  $\alpha \approx 0.1$ , with large fluctuations of all physical quantities. The inequality (1) is equivalent to the no torque inner boundary condition, or more precisely to a very small torque at the inner disk edge.

What can be wrong with eq. (1)? There are several possibilities. Thin disks, with  $H_{in}/r_{in} \ll 1$  may be physically impossible. We do not know if this is true or not, as we have neither theoretical nor observational proof either way. Steady state accretion may not exist in nature. Current 3-D simulations have demonstrated that strict steady state flow is

not possible, but there is a possibility that when averaged over moderate time scale a quasi steady state may still be a sensible approximation. The eq. (1) may hold as long as the fluctuating disk thickness remains always small. This domain is not accessible to numerical calculations so far. Next, there is a global problem pointed out by Abramowicz & Kato (1989): an accretion flow may pass through a sonic point near  $r_{ms}$  but it may not continue all the way into a black hole, as shown schematically in their Fig. 2. In fact, we could not find any reference from 1980s demonstrating that the supersonic infall for  $r < r_{ms}$  continues all the way. This was assumed to be obvious and the global flow pattern was not verified numerically.

Finally, there is an issue of terminology: what does it mean that the disk is geometrically thin? In the eq. (1) the disk thickness  $H$  refers to the structure which carries stresses. If the stresses which make the accretion possible are magnetic, as seems to be very likely, then  $H$  must refer to the geometrical thickness of the magnetic field structure, not just the gas layer. The notion that the magnetic thickness may be larger than gas thickness dates back at least to Galeev et al. (1979), and has found some support in recent 2-D and 3-D simulations. Even more importantly, all Blandford - Znajek type models are based on large scale magnetic structures to transfer momentum and energy. The distinction between the magnetic and gas disk structures was not considered at all in the classical papers about disk accretion, and it was not mentioned by Paczyński (2000). Yet, it is the scale height of the stresses that is important for eq. (1).

In this paper we present the simplest thin accretion disk model in order to demonstrate that there is no problem of the type envisioned by Abramowicz & Kato (1989), i.e. that once the infall becomes supersonic it never ‘turns back’. Our simple numerical model reproduces the basic features of classical thin disks, and demonstrates that the transonic solution may remain unique not only for a saddle, but also for a nodal critical point. But first we recall the simple concepts of the thin disk models of several decades ago. For the derivation of all equations the reader may consult the paper by Abramowicz & Kato (1989).

The single most important difference between Newtonian accretion and an accretion onto a black hole is the presence of a marginally stable orbit in the latter. Newtonian gravity varies strictly as a power of radius, therefore binding energy and the Keplerian angular momentum vary as a power law of radius, and this makes self-similarity an acceptable simplifying assumption for some accretion flows, including thin disks. This is not the case in general relativity: at small radii ‘Keplerian’ quantities are no longer power laws of radius, they do not even vary monotonically. The ‘Keplerian’ angular momentum and the corresponding binding energy reach a minimum at  $r_{ms}$ , the radius of a marginally stable orbit. This feature can be reproduced with a pseudo-Newtonian potential (Paczyński

& Wiita 1980):

$$\Psi = -\frac{GM}{r - r_g}, \quad r_g = \frac{2GM}{c^2}. \quad (2)$$

On a ‘Keplerian’ circular orbit we have a relation

$$\frac{d\Psi}{dr} = \frac{GM}{(r - r_g)^2} = \frac{v_K^2}{r}, \quad (3)$$

where  $v_K$  is the ‘Keplerian’ rotational velocity. It follows that ‘Keplerian’ angular momentum,  $l_K$ , angular velocity,  $\Omega_K$ , and binding energy,  $e_K$ , are given as

$$l_K = v_K r = (GMr)^{1/2} \left( \frac{r}{r - r_g} \right), \quad \Omega_K = \frac{v_K}{r} = \left( \frac{GM}{r^3} \right)^{1/2} \left( \frac{r}{r - r_g} \right), \quad (4a)$$

$$e_K = \Psi + \frac{v_K^2}{2} = -\frac{GM(r - 2r_g)}{2(r - r_g)^2} \quad (4b)$$

At very large radii,  $r/r_g \gg 1$ , the eqs. (2-4) asymptotically become Newtonian, but the differences are large at small radii. In particular, a minimum value of ‘Keplerian’ angular momentum and binding energy is reached at  $r = r_{ms} = 3r_g$ , just as it does in the relativistic Schwarzschild case. The orbits with  $r > r_{ms}$  are stable, while those with  $r < r_{ms}$  are unstable, with a marginal stability at  $r_{ms}$ .

Let us consider the simplest disk model with zero pressure. In this case all streamlines are identical with particle trajectories, i.e. they are nested ‘Keplerian’ orbits. This structure can be extended to small radii, but all orbits inwards of  $r_{ms}$  are unstable: a small perturbation makes a particle spiral into a black hole. Therefore, a zero pressure disk is truncated at  $r_{ms}$ , it cannot extend inwards of  $r_{ms}$ . Such a disk has zero geometrical thickness, and it is static, i.e. there is no accretion.

To make disk accretion possible it is necessary to introduce some means of angular momentum exchange between nearby streamlines. In general, this will require a non-zero pressure  $P$ , a non-zero speed of sound  $v_s \approx (P/\rho)^{1/2}$ , and a small disk thickness  $H$ . For simplicity we assume the speed of sound to be constant:

$$\frac{H}{r} \approx \frac{v_s}{v_K} \ll 1, \quad v_s = const, \quad \frac{v_s^2}{c^2} \approx \frac{P}{\rho c^2} \ll 1, \quad \Sigma = \int \rho dz, \quad (5)$$

As is conventional, we assume that the stresses responsible for angular momentum transport are proportional to pressure ( $P$ ) and shear rate. The torque exerted across radius  $r$  by these stresses is

$$g = -\alpha 2\pi r^2 \Omega_K^{-1} \left( \frac{d\Omega}{d \ln r} \right) \int P dz = -\alpha 2\pi r^2 \left( \frac{d \ln \Omega}{d \ln r} \right) \left( \frac{\Omega}{\Omega_K} \right) v_s^2 \Sigma. \quad (6)$$

The dimensionless factor  $\alpha$  is assumed to be less than unity, and for simplicity we take it to be constant. A wide variety of physical transport mechanisms can be parameterized in this way, especially in steady disks, and especially if  $\alpha$  is allowed to be a more general function of the state of the disk. Note, that  $\Omega$  varies monotonically with radius, i.e. the inner disk rotates faster, and angular momentum is transported outwards.

The  $\alpha P$  term, no matter how small, redistributes angular momentum within the disk, and accretion becomes possible. In a steady state each disk element gradually loses its angular momentum, and slowly spirals inwards. For  $r > r_{ms}$  the process can be envisioned as a motion along ever smaller nearly ‘Keplerian’ orbits, with gradually decreasing angular momentum. This will bring matter close to  $r_{ms}$ . Following any additional loss of angular momentum the gas cannot find any ‘Keplerian’ orbit and must plunge into the black hole along a spiral, approximately conserving angular momentum.

Let us assume a steady state, with the mass accretion rate  $\dot{M} = const < 0$ , and the radial flow velocity  $v_r < 0$  assumed to be a function of radius only. The conservation laws of mass and angular momentum are

$$\dot{M} = 2\pi r \Sigma v_r, \quad g = (-\dot{M}) (l - l_0), \quad (7)$$

where  $l_0$  is the integration constant (cf. Abramowicz & Kato 1989). Combining eqs. (6) and (7) we obtain

$$(-v_r) (l - l_0) = \alpha r v_s^2 \left( -\frac{d \ln \Omega}{d \ln r} \right) \left( \frac{\Omega}{\Omega_K} \right). \quad (8)$$

It is reasonable to expect that  $l_0 \approx l_{ms}$  (to be verified later), and the last equation may be used to estimate the radial flow velocity in the nearly ‘Keplerian’ thin disk for  $r > r_{ms}$  and  $|v_r|/v_s \ll 1$ .

Note, that in eq. (8) only two quantities vary a lot within the flow:  $v_r$  and  $(l - l_0)$ , while the others are either constant or vary slowly. In particular, according to the classical theory of thin accretion disks, near the  $r_{ms}$  and inwards of  $r_{ms}$  angular momentum is almost conserved. This implies that

$$\left( -\frac{d \ln \Omega}{d \ln r} \right) \approx 2, \quad \text{and} \quad (-v_r) (l - l_0) \approx 2\alpha r v_s^2 \left( \frac{\Omega}{\Omega_K} \right). \quad (9)$$

We shall verify this assertion with our numerical model.

When matter reaches  $r \approx r_{ms}$  any additional loss of angular momentum puts it on a spiral infall towards the black hole, during which energy and angular momentum are approximately conserved, i.e.

$$e = -\frac{GM}{r - r_g} + \frac{v_r^2}{2} + \frac{v_{rot}^2}{2} \approx e_{ms} = -\frac{c^2}{16}, \quad l = v_{rot} r \approx l_{ms} = 3\sqrt{1.5} \frac{GM}{c}, \quad (10)$$

where  $v_{rot}$  is the rotational velocity component of the infall.

To calculate a transition from the subsonic radial flow to the supersonic flow we need the equation of motion (cf. Abramowicz & Kato 1989)

$$v_r \frac{dv_r}{dr} - (\Omega^2 - \Omega_K^2) r + \frac{v_s^2}{\Sigma} \frac{d\Sigma}{dr} + v_s^2 \frac{d \ln \Omega_K}{dr} = 0. \quad (11)$$

Differentiating the mass conservation law (eq. 7) we obtain

$$\frac{v_s^2}{\Sigma} \frac{d\Sigma}{dr} = -\frac{v_s^2}{r} - v_s^2 \frac{d \ln v_r}{dr}, \quad (12)$$

and combining eqs. (11) and (12) we find

$$(v_r^2 - v_s^2) \frac{d \ln v_r}{d \ln r} - (\Omega^2 - \Omega_K^2) r^2 + v_s^2 \left( \frac{d \ln \Omega_K}{d \ln r} - 1 \right) = 0. \quad (13)$$

We introduce dimensionless constants and variables defined as

$$a \equiv \frac{v_s}{c} \ll 1, \quad b \equiv \frac{l_0}{l_{ms}} \approx 1, \quad 0 < \alpha < 1, \quad (14a)$$

$$\omega \equiv \frac{\Omega}{\Omega_K}, \quad v \equiv -\frac{v_r}{c} > 0, \quad x \equiv \frac{r}{r_g}. \quad (14b)$$

The equation of motion (13) and conservation of angular momentum (9) may be written in dimensionless form as

$$\frac{d \ln v}{d \ln x} = \frac{1}{(v^2 - a^2)} \left[ (\omega^2 - 1) \frac{x}{2(x-1)^2} + 2.5 a^2 \frac{x-0.6}{x-1} \right], \quad (14)$$

$$\omega = \frac{1.5\sqrt{3} b(x-1)v}{x [x^{1/2}v - 2\sqrt{2} \alpha a^2(x-1)]}, \quad (15)$$

### 3. Critical Points, Physical Solutions and their Topology

We seek a physical solution which has the properties

$$v/a \ll 1, \quad \omega \approx 1, \quad \text{for } x \gg 3, \quad (16a)$$

$$v = a, \quad \text{for } x = x_c \approx 3, \quad (16b)$$

$$v/a \gg 1, \quad \text{for } x \ll x_c. \quad (16c)$$

i.e. the flow is subsonic and the disk is ‘Keplerian’ at large radii, the flow passes through a critical point near the marginally stable orbit, and it becomes supersonic at small radii.

To better understand the behavior of the physical solutions of eq. (14), and to be able to integrate it numerically near the critical point, we decompose it into two equations

$$\frac{d \ln v}{dt} = (\omega^2 - 1) \frac{x}{2(x-1)^2} + 2.5 a^2 \frac{x - 0.6}{x - 1}, \quad (17a)$$

$$\frac{d \ln x}{dt} = v^2 - a^2, \quad (17b)$$

which, together with eq. (15), form a two-dimensional autonomous dynamical system. The variable  $t$ , is a dummy variable and should not be confused with the physical time.

As mentioned earlier, the physical solution must pass a critical point to reach the supersonic regime, otherwise the solution would not be single-valued as the right hand side of eq. (14) diverges. Now, the critical points of eq. (14) are the fixed points of eqs. (17) and an understanding of the nature of these fixed points is necessary for constructing a physical solution.

At any fixed point, the right hand sides of eqs. (17) vanish. Eq. (17b) implies that fixed points are always at  $v = a$ , as required by eq. (16b). The right hand side of eq. (17a) at the critical point, together with eq. (15) (with  $v = a$ ) lead to a complicated algebraic equation for  $x$  at a given  $b$ , or vice versa. The analysis is significantly simplified for small values of  $a$  and the corresponding relation between  $b$  and  $x_c$  is shown in Fig. 1. We see that, in general, there are either no fixed points or two fixed points in the system, while at the critical value of  $b = 1 + O(\alpha a)$ , there is only a single degenerate fixed point at  $x \approx 3$ .

The nature of the fixed points can be investigated analytically by linearizing eqs. (17) around each of them. It turns out that the left fixed point (smaller value of  $x$ ) is always saddle-like, i.e. the two eigenvalues have opposite signs. The right fixed point is of the spiral type (two complex eigenvalues) when the two fixed points are far apart, but it switches to the nodal type (two eigenvalues of the same sign) as the two fixed points get closer. This behavior is shown in Figs. 2-5 which is the typical behavior of a saddle-node bifurcation (Guckenheimer & Holmes 1983).

The integrations presented in Figs. 2-5 were calculated numerically, except near the critical points, where an analytic expansion was used. All four figures have the same disk parameters:  $a = v_s/c = 0.01$  and  $\alpha = 0.15$ . They differ in the adopted value of the angular momentum constant  $b$ . The family of solid lines shown in each figure represents possible solutions of the eq. (14). The solutions of special interest for us are those which satisfy

boundary conditions (16a,b,c). As it turns out none of these figures has a desired solution, but the figures present the changes in the structure of the critical points.

Fig. 2 presents a saddle critical point at  $x_c = 2.7$ , and a spiral point at  $x_c = 3.4$ . The Phase Portraits for  $b > 0.9997$  (including  $b > 1$ ) is qualitatively similar to Fig. 2. The Phase Portrait changes when the angular momentum constant  $b$  is reduced, as shown in Fig. 3, where the two critical points are saddle at  $x_c = 2.94$ , and nodal at  $x_c = 3.1$ . When  $b$  is reduced down to  $b = 0.9947$  the two critical points merge, as shown in Fig. 4. This corresponds to the point marked  $(x_c, 1)$  in Fig. 1. When  $b$  is reduced even more then there is no critical point, as demonstrated with Fig. 5, and as was anticipated (cf. Fig. 1).

A prominent feature of Figs. 2-5 is the ‘Keplerian’ solution. In the subsonic regime, ( $v \ll a$ ), the the right hand side of eq. (14) is very large for small values of  $a$  unless  $\omega \simeq 1$  (almost ‘Keplerian’ angular velocity). This implies that the only slowly varying solution of eq. (14) is an almost ‘Keplerian’ one. The radial velocity for a ‘Keplerian’ solution is obtained by setting  $\omega = 1$  in eq. (15),

$$v_0 = \frac{2\sqrt{2}\alpha a^2 x}{x^{3/2}/(x-1) - 3\sqrt{3}b/2} + O(a^4). \quad (18)$$

Figs. 2-5 show that all the other solutions tend to merge with the ‘Keplerian’ solution as  $x$  decreases. This implies that the behavior of the physical solution close to  $r_{ms}$  is independent of the boundary condition at large radii, since all different solutions merge as they move inwards. Therefore, it is easy to satisfy the boundary condition given with eq. (16a). However, none of the solutions shown in Figs. 2-5 satisfies all three conditions given by eqs. (16a,b,c).

It is clear that a physical solution may pass through a saddle or a nodal fixed point, but not a spiral. Furthermore, we assume that a physical solution is analytic. This singles out only two ways of passing a nodal fixed point (slow or fast modes), because a linear superposition of fast and slow modes is non-analytic (when  $v$  is expressed as a function of  $x$ ). In the case of a saddle fixed point, only two solutions (in the direction of two eigenvectors) can pass the fixed point. A conclusion that can be drawn from this consideration is that, in general, the ‘Keplerian’ solution does not analytically pass the fixed points and only for discrete values of the angular momentum constant  $b$  a physical solution is possible.

Now, we are ready to analyze different topologies that can occur in the parameter space of our model. For a given value of  $a$  the nature of critical points can be calculated analytically for any pair of values of  $\alpha$  and  $x_c$ , or equivalently  $\alpha$  and  $b$ . Fig. 6 shows the possibilities for  $a = v_s/c = 0.01$ . The horizontal axis,  $x$ , is the position of a fixed point and the vertical axis is the parameter  $\alpha$  that appears in the viscosity model (eq. 5). The fixed

points are of the saddle-type, on the left side of the dashed region, of the nodal type inside the dashed region, and of the spiral type on the right side of the dashed region. The solid curve aBCd shows the position of physical solutions that allow passage of the ‘Keplerian’ curve through the critical point. The critical points present in Figs. 2-4 are indicated in Fig. 6 with diamonds numbered 2, 3, 4, 3, and 2, correspondingly, with  $\alpha = 0.15$  for all of them. The diamonds with numbers 7, 9, and 11, correspond to critical points presented in Figs. 7, 9, 11; they are all located on the solid line aBCd.

We note that for  $\alpha$  smaller than some critical value  $\alpha_{SN}$ , the physical critical point is of the saddle type (segment aB), while for larger values of  $\alpha$  it is of the nodal type (segment Bd). The value of  $\alpha_{SN}$  depends on  $a$ . For example for  $a = 0.01$  we have  $\alpha_{SN} = 0.08$  (cf. Fig. 6).

A critical point of the saddle type, shown in Figs. 7 and 8, is the type that is usually encountered in astrophysics. The best known examples are the solar wind (Parker 1958) and Roche lobe overflow in binary stars. As argued above, when the parameters  $a$  and  $\alpha$  are fixed then physical solution exists only for a unique value of  $b$  and the corresponding value of  $x_c$ .

In the case of a nodal critical point, the passage is possible through fast or slow directions. However, a generic solution, which is a combination of fast and slow modes, passes the critical point in the slow direction since the slow solution dominates the fast one close to the critical point. In this sense, a physical solution that passes a nodal point in the fast direction, is unique, similar to the saddle critical point. This kind of passage is seen in the BC section of the aBCd curve in Fig. 6 and an example of the phase portrait is shown in Figs. 9 and 10. Note that, again similar to the saddle point solutions, there is a smooth transition from the subsonic to the supersonic regime.

Finally, the physical solution may pass the critical point in the slow direction. However, as argued above, this does not fix the value of  $b$  since it is the generic behavior of the solutions, and only by requiring the analyticity of the physical solution may one determine  $b$  uniquely. The reason is that only pure fast or slow solutions are smooth, while a combination of them, although it merges with the slow solution close to the critical point, is not so smooth. The points on the Cd segment in Fig. 6 are of this type, and an example of the phase portraits is plotted in Figs. 11 and 12.

The transition from the former type of nodal passage to the latter occurs at  $\alpha_{NN}$ . For example, for  $a = 0.01$ ,  $\alpha_{NN} \simeq 0.14$  (point C in Fig. 6). The curve aBCd, at the transition point C, is tangent to the boundary of the nodal and saddle regions, where the fast and slow directions merge.

The main difference between the last type of passage and the previous two types is that there is a sharp change in slope, right after passing the critical point. The reason is that the ‘Keplerian’ curve, which is connected to the slow direction, turns from stable (as  $x$  decreases) in the subsonic regime to unstable in the supersonic regime, and so the physical solution departs from the ‘Keplerian’ curve after the passage. Since the slopes are significantly larger far from the ‘Keplerian’ curve, there is a sharp change in slope.

#### 4. Some Analytic Results

In order to have an analytic understanding of the behavior of the solutions and the dependence on the parameters  $\alpha$  and  $a$  we attempt to replace eq. (14) by a simplified version of it, which retains the main topological features of the phase portrait, i.e. critical points and the ‘Keplerian’ curve, and also the dependence on  $\alpha$  and  $a$  for small  $a$ ’s. First let us define  $\nu = v/a$  and  $\nu_0 = v_0/a$ , where  $v_0$ , defined in eq.(18), is the ‘Keplerian’ radial velocity. Next we make the following assumptions

$$x \simeq 3, \nu_0 \simeq 1, \omega \simeq 1, \quad (19)$$

which all follow from the assumption of  $a \ll 1$  and restricting the study to the vicinity of the ‘Keplerian’ curve (that includes the critical points). After these substitutions, being careful not to drop terms that are crucial for the main topological features, we end up with

$$\frac{d\nu}{dx} \simeq -\frac{\alpha(\nu - \nu_0)}{\sqrt{6}a\nu_0(\nu - 1)}. \quad (20)$$

We see that the ‘Keplerian’ curve, for which  $d\nu/dx$  vanishes, and the critical points, where  $\nu = \nu_0 = 1$ , are preserved.

Next, we try to find a workable approximation for  $\nu_0(x)$ . To do so, we notice that the interesting transitions in the nature of the physical solution (Fig. 6) happens where the critical points are close to the maximum of  $\nu_0(x)$ , which is also close to 1. With these approximations, we can use eq. (18) to get

$$\frac{d \ln \nu_0}{dx} \simeq \frac{d\nu_0}{dx} \simeq 1/3 - 2B(x - 3), \quad (21)$$

where

$$B^{-1} = 32\sqrt{6}\alpha a, \quad (22)$$

which can be integrated to give

$$\nu_0(x) \simeq 1 + B[(x_c - x_b)^2 - (x - x_b)^2], \quad x_b = 3 + B^{-1}/6. \quad (23)$$

$x_c$  is the position of the critical point, which is related to  $b$  by setting  $\omega = 1$  in eq.(15), and  $x_b$  is the Saddle-Node bifurcation point, the boundary of the Saddle region and the Nodal region in Fig. 6.

Now, let us define the new variables  $\xi$ ,  $\Delta$  and  $\mu$

$$\xi \equiv B^{1/2}(x - x_b), \quad \mu \equiv B^{1/2}\sqrt{6}a/\alpha = \left[\frac{\sqrt{6}a}{32\alpha^3}\right]^{1/2}, \quad \Delta \equiv \nu - \nu_0. \quad (24)$$

In terms of these new variables, eq.(20) becomes

$$\frac{d\Delta}{d\xi} = -\frac{\mu^{-1}\Delta}{(1 + \xi_c^2 - \xi^2)(\Delta + \xi_c^2 - \xi^2)} + 2\xi. \quad (25)$$

Now, it is easy to find the eigenmodes  $M$  of the critical point, by setting  $\Delta$  equal to  $M(\xi - \xi_c)$  and requiring that it satisfies eq. (25) to the first order in  $\xi - \xi_c$ . This yields

$$M = -\frac{1}{2\mu}(1 - 4\mu\xi_c \pm \sqrt{1 - 8\mu\xi_c}), \quad (26)$$

which already gives the three saddle, nodal and spiral regions in Fig. 6.

We do not intend to elaborate any further on the behavior of the solutions of eq.(25). This is mainly because the main property of the physical solution which is connecting the asymptotically ‘Keplerian’ curve to the critical point, is a global property and so its analytical investigation is not straightforward. The only clear conclusion that we can draw from eq.(25) is that the value of  $\xi_c$  for which the physical solution exists is a function of  $\mu$ . The transitions in the nature of the critical point, points B (SN) and C (NN) in Fig. 6, that were discussed in the last section, occur at specific values of  $\mu$  which can be already fixed from the numerical results in Fig. 6 and the definition of  $\mu$  in eq. (24)

$$\mu_{SN} \simeq 1.22, \quad \mu_{NN} \simeq 0.53. \quad (27)$$

Of course the advantage is that now we can apply this result to all small values of  $a$  and not only  $a = 0.01$ . This yields

$$\begin{aligned} \left(\frac{a}{0.01}\right) &< \left(\frac{\alpha}{0.14}\right)^3, && \text{Nodal Point Through Slow Direction,} \\ \left(\frac{\alpha}{0.14}\right)^3 &< \left(\frac{a}{0.01}\right) < \left(\frac{\alpha}{0.08}\right)^3, && \text{Nodal Point Through Fast Direction,} \\ \left(\frac{\alpha}{0.08}\right)^3 &< \left(\frac{a}{0.01}\right), && \text{Saddle Point.} \end{aligned} \quad (28)$$

The numerical values calculated for  $a = 0.02$  agree very well with these scalings.

## 5. Discussion

After numerical and analytical study of the properties of the solutions of eq. (14) in the last two sections, we are now ready to discuss the physical picture within the framework of our approximations. Of course the question of the accuracy of these approximations should be addressed as well, and we intend to do so, at least in part.

### 5.1. Torque at the Sonic Point

The starting point of this investigation was a recent controversy about the significance of the torque at the sonic point of the accretion disk. The traditional picture of Novikov & Thorne (1973) which suggests a zero torque boundary condition at the marginally stable orbit  $r_{ms}$  is challenged by Krolik (1999), Gammie(1999), Agol & Krolik(2000) and later by the MHD global disk simulations (e.g. Hawley et al. 2001, Armitage et al. 2001) which also show large temporal and spatial variations in basically all the properties of the disk and even outflows (Flemming et al. 2000, Hawley et al. 2001, Armitage 2001a,b, Armitage et al. 2001, Reynolds & Armitage 2001, Reynolds et al. 2001, Sano & Inutsuka 2001).

It is easy to verify the validity of the traditional view in our picture. Eq.(7) says that the magnitude of the torque is proportional to  $(l - l_0)$  and eq.(9) gives  $l - l_0$  as a function of  $r$  and  $v$ . Let us find the ratio of  $g$  of the sonic point at  $r_c \simeq r_{ms}$ , to  $g$  at, say  $10r_{ms}$ . We assume to have a ‘Keplerian’ radial velocity at  $10r_{ms}$  (eq. (18)) and  $b \simeq 1$ , as seen in Section 3.

$$\frac{g(r_{ms})}{g(10r_{ms})} \simeq 3\alpha a \ll 1, \quad a = v_s/c. \quad (29)$$

Indeed, since  $g \propto (l - l_0) \propto v^{-1}$ ,  $g$  drops steeply as  $v$  rises steeply close to the critical point (e.g. see Figs. 7, 9 and 11).

Of course this result is valid, only in the framework of our approximations, most crucially the assumption that the disk is thin and the accretion is steady. The numerical MHD simulations of slim disks  $H/r \sim 0.1$  hardly falls in this category: they are not thin, and they show rapid fluctuations in all physical quantities. However, all recent 3-D time dependent numerical models (Flemming et al. 2000, Hawley et al. 2001, Armitage 2001a,b, Armitage et al. 2001, Reynolds & Armitage 2001, Reynolds et al. 2001, Sano & Inutsuka 2001) neglect cooling processes, while an efficient cooling is the essential reason for the gas relaxing into a thin disk, and in its absence the gas tends to heat up to the virial temperature. Also, none of the numerical simulations was carried out over large range of radii and over time much longer than disk rotation time, and little is known about the

fluctuations averaged over a very long time. It is not clear if the fluctuations found in the numerical simulations would remain equally strong if cooling processes were allowed for. It is also not clear if the time averaged torque at  $r_{ms}$  would be affected by the fluctuations if the disk remained geometrically thin at  $r_{ms}$  at all time. We consider it likely that the time averaged inequality (29) would remain valid if the disk remained geometrically thin, while fluctuating in time.

Although some of the assumptions used in the derivation of eq. (29) may turn out to be incorrect, and the torque at the inner disk boundary may turn out to be large, we have not seen any convincing argument/paper that disproves the claim that that torque is very small if the disk is geometrically thin.

## 5.2. Is constant $v_s$ a good approximation?

Obviously, no flow is strictly isothermal, and the real question is: does the isothermal flow capture the essential properties of thin disk accretion? A specific issue, brought up by Krolik (1999), Gammie (1999) and Agol & Krolik (2000), was the possibility that the differential rotation within the supersonic flow will increase the speed of sound to a significant fraction of the speed of light, i.e. the temperature and the speed of sound will increase very strongly.

Let us estimate the maximum amount of energy that may be released due to shear flow. The energy input per unit area, i.e. integrated over thin disk thickness, is given with a standard formula

$$2F_+ = \frac{g}{2\pi r} \left( -\frac{d\Omega}{dr} \right) = (-\dot{M}) \frac{l - l_0}{2\pi r} \left( -\frac{d\Omega}{dr} \right) \left( \frac{\Omega}{\Omega_K} \right), \quad (30)$$

(c.f. eqs. 6, 7). The total amount of energy released within the supersonic stream can be estimated as follows (cf. eq. 9):

$$\begin{aligned} L_+ &\equiv \int_r^{r_{ms}} 2F_+ 2\pi r dr = (-\dot{M}) \int_r^{r_{ms}} (l - l_0) \left( -\frac{d\Omega}{dr} \right) \left( \frac{\Omega}{\Omega_K} \right) dr \approx \\ &2 (-\dot{M}) l_{ms} \int_r^{r_{ms}} \frac{l - l_0}{r^3} \left( \frac{\Omega}{\Omega_K} \right) dr < (-\dot{M}) l_{ms} (l - l_0)_{ms} \left( \frac{1}{r^2} - \frac{1}{r_{ms}^2} \right) = \\ &(-\dot{M}) \frac{2\alpha l_{ms} v_s}{r_{ms}} \left( \frac{r_{ms}^2}{r^2} - 1 \right) \approx (-\dot{M}) \sqrt{1.5} \alpha a c^2 \left( \frac{r_{ms}^2}{r^2} - 1 \right) \\ &\approx (-\dot{M}) \frac{c^2}{100} \left( \frac{\alpha}{0.1} \right) \left( \frac{a}{0.01} \right) \left[ \left( \frac{r_g}{r} \right)^2 - \frac{1}{9} \right] < (-\dot{M}) \frac{c^2}{100} \left( \frac{\alpha}{0.1} \right) \left( \frac{a}{0.01} \right), \end{aligned} \quad (31)$$

as  $r_{ms} > r > r_g$ . This is to be compared with the energy released within the disk:

$$L_d = (-\dot{M}) e_{ms} = (-\dot{M}) \frac{c^2}{16}, \quad (32)$$

(cf. eq. 10). It is clear that for a thin disk ( $a = 0.01$ ) even a very generous upper limit to the energy that shear may deposit within the supersonic flow is significantly smaller than the energy deposited within the disk itself, i.e. within the subsonic accretion flow. In other words, the speed of sound cannot become relativistic for  $r < r_{ms}$ . Obviously, the reasoning presented above does not apply to slim or thick disks.

### 5.3. Is Nodal Passage in the Slow Direction Physical?

Inspection of Figs. 2, 3, 4, 7, 8, 9, and 10 shows that the geometry of transonic flow appears to be similar when the critical point is of a saddle type or a nodal type, provided the solution passes the latter in the fast direction. The transition from the saddle to the nodal (fast) geometry is smooth, with no apparent problem. The subsonic flow connects well to a ‘Keplerian’ disk at large radii, and the supersonic flow approaches a free fall at small radii. This trouble free region corresponds to the thick line in Fig. 6, and this ends at point C, where it contacts the borderline of the fixed points of the spiral type, and where  $\alpha = 0.14$ . Obviously, no physical solution can pass through a spiral point. Above point C the analytical solutions pass the nodal critical point in the slow direction, and these solutions do not appear to be physical (cf. Fig. 11), as there is a sharp change in the slope of the physical solution (see the end of Sec. 3). We do not know if they are unstable, or perhaps no truly steady-state isothermal flow is possible for  $\alpha > 0.14$  (for  $a = 0.01$ ).

## 6. Conclusions

We have demonstrated that an isothermal, steady state accretion disk, with given speed of sound  $v_s = 0.01c$ , and a given viscosity parameter  $\alpha < 0.14$ , has a unique transonic solution, with a saddle or nodal (fast) sonic point located near the marginally stable orbit, at  $r_{in} \approx r_{ms}$ . The torque at the sonic point is very small (cf. eq. 1), and hence the so called ‘zero torque’ inner boundary condition is a good approximation for geometrically thin disks. We emphasize that the disk thickness  $H$  must include the thickness of magnetic structures responsible for angular momentum transfer, not just the thickness of the gas layer. While our numerical solutions are for an isothermal flow only, it is very likely that the only important condition for the correctness of the ‘zero torque’ condition at  $r_{in}$  is the requirement that the disk thickness be small there,  $H_{in}/r_{in} \ll 1$ .

It is a great pleasure to acknowledge many useful and critical comments by Dr. J. Goodman.

## REFERENCES

- Abramowicz, M. A., Jaroszyński, M. & Kozłowski, M. 1978, *A&A*, 63, 209
- Abramowicz, M. A., & Kato, S. 1989, *ApJ*, 336, 304
- Agol, E., & Krolik, J. H. 2000, *ApJ*, 528, 161
- Agol, E., Krolik, J., Turner, N. J. & Stone, J. M. 2001, *ApJ*, 558, 543
- Armitage, P. J. 1998, *ApJ*, 501, L189
- Armitage, P. J. 2001, *astro-ph/0110250*
- Armitage, P. J. 2001, *astro-ph/0110670*
- Armitage, P. J. & Natarajan, P. 1999, *ApJ*, 523, L7
- Armitage, P. J., Reynolds, C. S. & Chiang, J. 2001, *ApJ*, 548, 868
- Balbus, A. S. & Hawley, J. F. 1991, *ApJ*, 376, 214
- Ball, G. H., Narayan, R. & Quataert, E. 2001, *ApJ*, 552, 221
- Blandford, R. D. & Znajek, R. L. 1977, *MNRAS*, 179, 433
- Cunningham, C. T. 1975, *ApJ*, 202, 788
- Cunningham, C. T. 1976, *ApJ*, 208, 534
- Flemming, T. P., Stone, J. M. & Hawley, J. F. 2000, *ApJ*, 530, 464
- Galeyev, A. A., Rosner, R. & Vaiana, G. S. 1979, *ApJ*, 229, 318
- Gammie, C. F. 1999, *ApJ*, 522, L57
- Guckenheimer, J., Holmes, P., “Nonlinear Oscillations, Dynamical Systems, and Bifurcation of Vector Fields”, 1983, Springer
- Hawley, J. F. & Balbus, A. S. 1991, *ApJ*, 376, 223
- Hawley, J. F., Balbus, S. A., & Stone, J. M. 2001, *ApJ*, 554, L49
- Krolik, J. H. 1999, *ApJ*, 515, L73
- Li, L.-X. 2000a, *ApJ*, 531, L111
- Li, L.-X. 2000b, *ApJ*, 533, L115
- Lin, D. N. C. & Papaloizou, J. C. B. 1996, *ARA&A*, 34, 205

- Livio, M., Oglive, G. L. & Pringle, J. E. 1999, *ApJ*, 512, 100
- Lynden-Bell, D. & Pringle, J. E. 1974, *MNRAS*, 168, 603
- Muchotrzeb, B. & Paczyński, B. 1982, *AcA*, 32, 1
- Novikov, I. D. & Thorne, K. S. 1973, In ‘Black Holes - Les Astres Occlus’, Eds: C. De Witt & B. S. De Witt, New York: Gordon & Breach
- Paczyński, B. 2000, *astro-ph/0004129*
- Paczyński, B., & Wiita, P. 1980, *A&A*, 88, 23
- Parker, E. N. 1958, *ApJ*, 128, 664
- Pringle, J. E. 1981, *ARA&A*, 19, 137
- Pringle, J. E. & Rees, M. J. 1972, *A&A*, 21, 1
- Reynolds, C. S. & Armitage, P. J. 2001, *ApJ*, 561, L81
- Reynolds, C. S., Armitage, P. J. & Chiang, J. 2001, *astro-ph/0102045*
- Sano, T. & Inutsuka, S.-I. 2001, *ApJ*, 561, L179
- Shakura, N. I. & Sunyayev, R. A. 1973, *A&A*, 24, 337
- Stoeger, W. R. 1976, *A&A*, 53, 267
- Stone, S. & Pringle, J. E. 2001, *MNRAS*, 322, 461
- Stone, J. M., Pringle, J. E. & Begelman, M. C. 1999, *MNRAS*, 310, 1002
- Wilms, J. et al. 2001, *MNRAS*, 328, L27

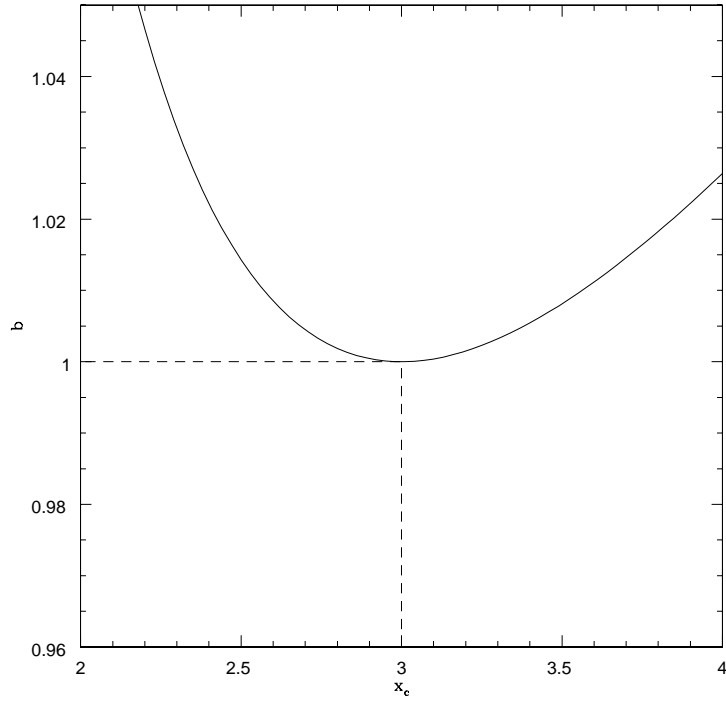


Fig. 1.— The angular momentum constant  $b$  is shown as a function of the position of the critical point  $x_c$  for  $a \rightarrow 0$ . We see that, for  $b > 1$ , there are two fixed points, at  $b = 1$ , there is one degenerate fixed point at  $x = 3$  (marginally stable orbit), and for  $b < 1$  no fixed point exist.

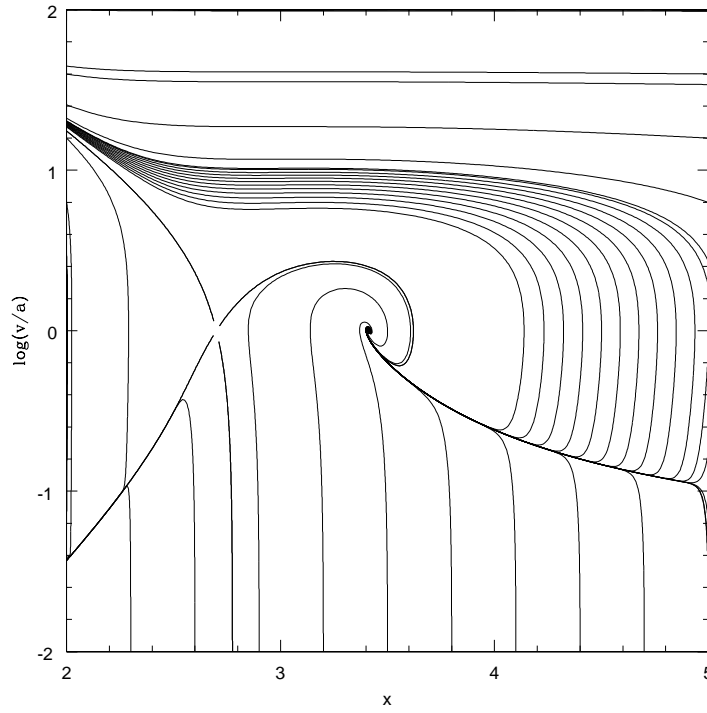


Fig. 2.— The Phase Portrait for  $a = 0.01, \alpha = 0.15$  and  $b = 0.9997$ . There is a saddle point at  $x = 2.7$  and a spiral point at  $x = 3.4$ .

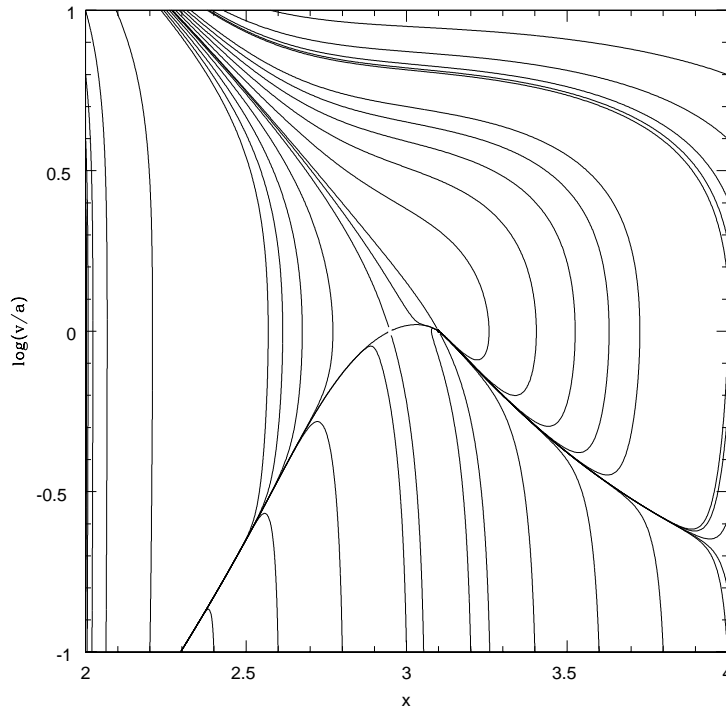


Fig. 3.— The Phase Portrait for  $a = 0.01, \alpha = 0.15$  and  $b = 0.9949$ . There is a saddle point at  $x = 2.94$  and a nodal point at  $x = 3.1$ .

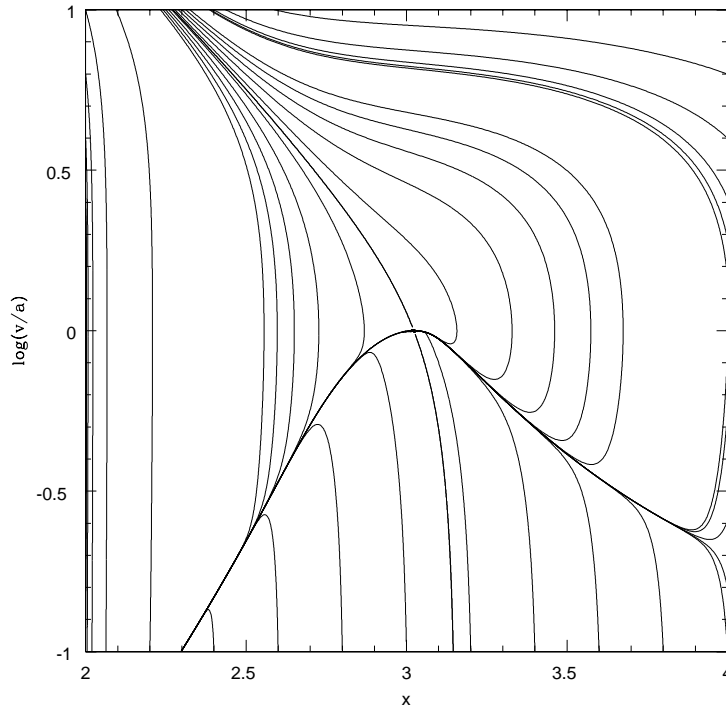


Fig. 4.— The Phase Portrait for  $a = 0.01$ ,  $\alpha = 0.15$  and  $b = 0.9947$ . There is a degenerate saddle-node point at  $x = 3.0228$ .

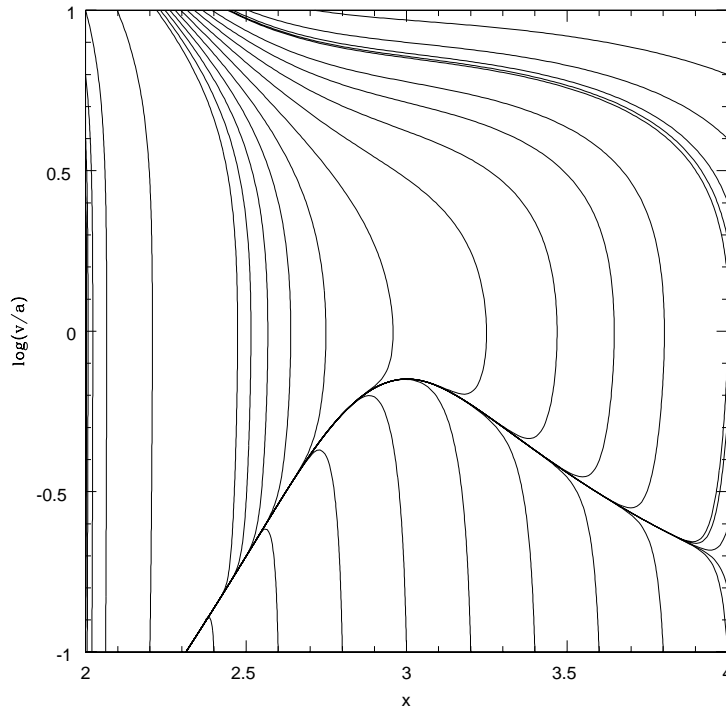


Fig. 5.— The Phase Portrait for  $a = 0.01$ ,  $\alpha = 0.15$  and  $b = 0.9927$ . There is no fixed point for these parameters.

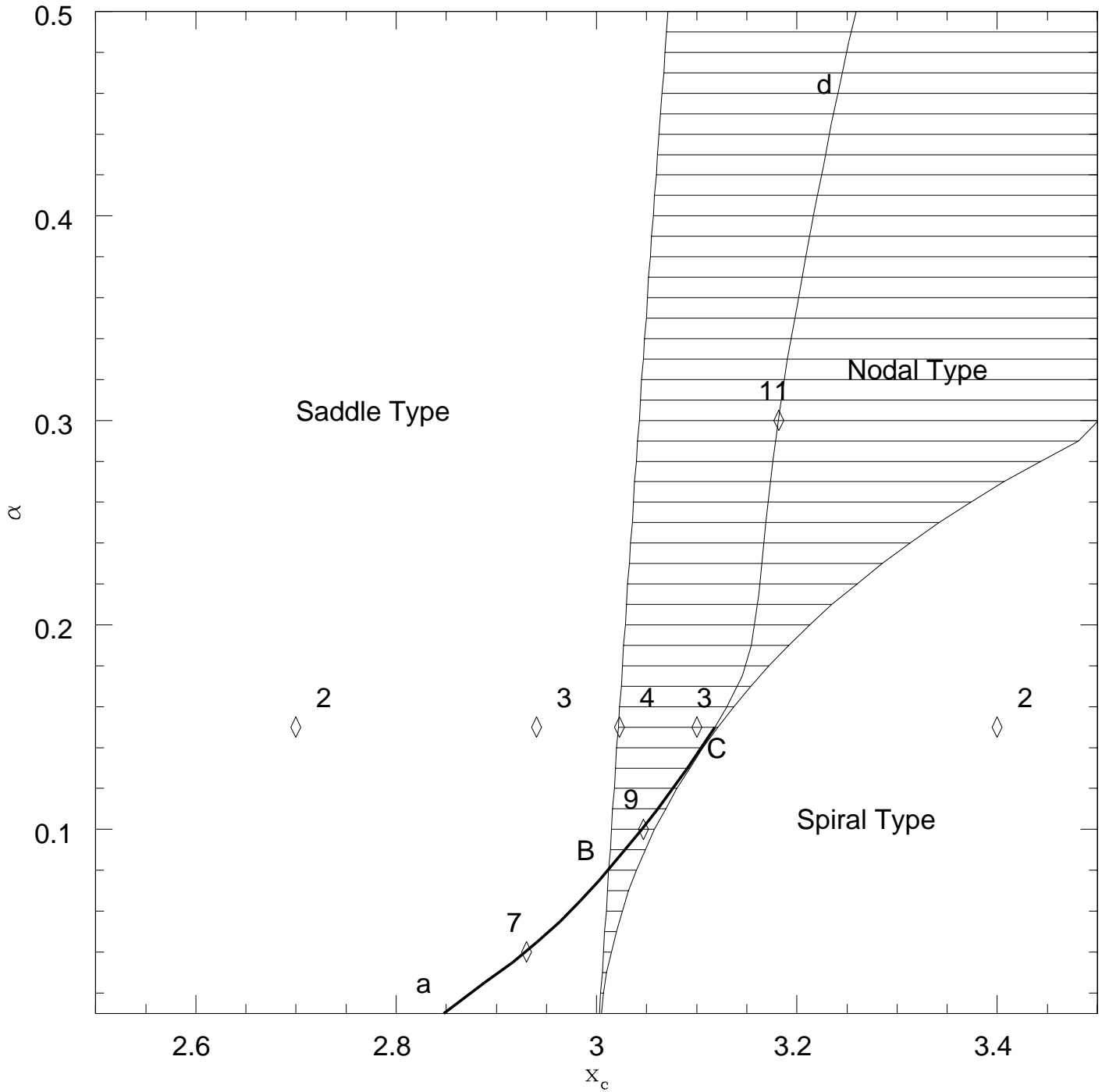


Fig. 6.— The parameter space of the problem for  $a = v_s/c = 0.01$ .  $x_c$  is the radius of the critical point in units of  $r_g$  and  $\alpha$  is the viscosity parameter. The curve aBCd shows the position of the fixed points that allow physical solutions. Also the parameters of phase portraits in the other figures are represented by numbered diamonds. The number of each diamond is the number of the associated figure in this paper. The Phase Portrait presented in Fig. 5 has no fixed points, and therefore it is not represented in this figure.

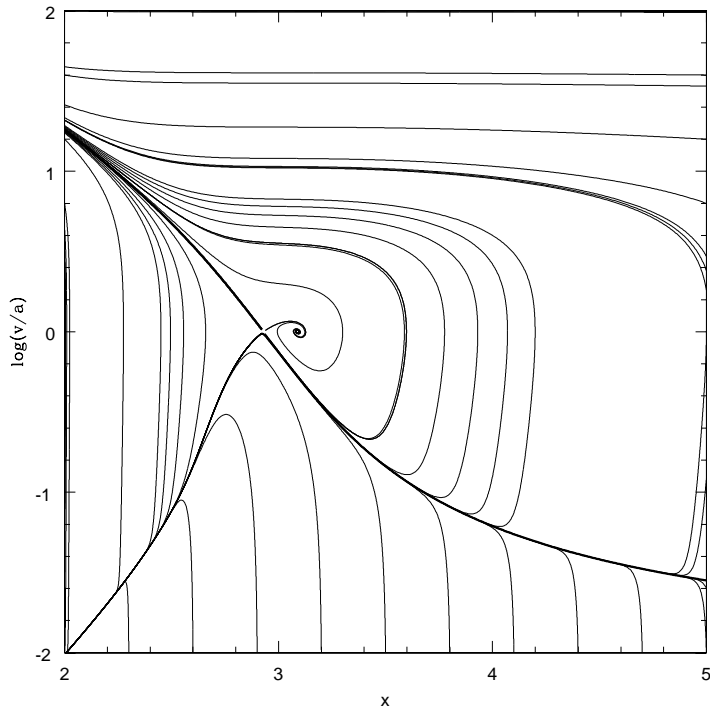


Fig. 7.— The Phase Portrait for  $a = 0.01, \alpha = 0.04$  and  $x_c \simeq 2.930$ . The physical solution (thick curve) passes a critical point of the saddle type.

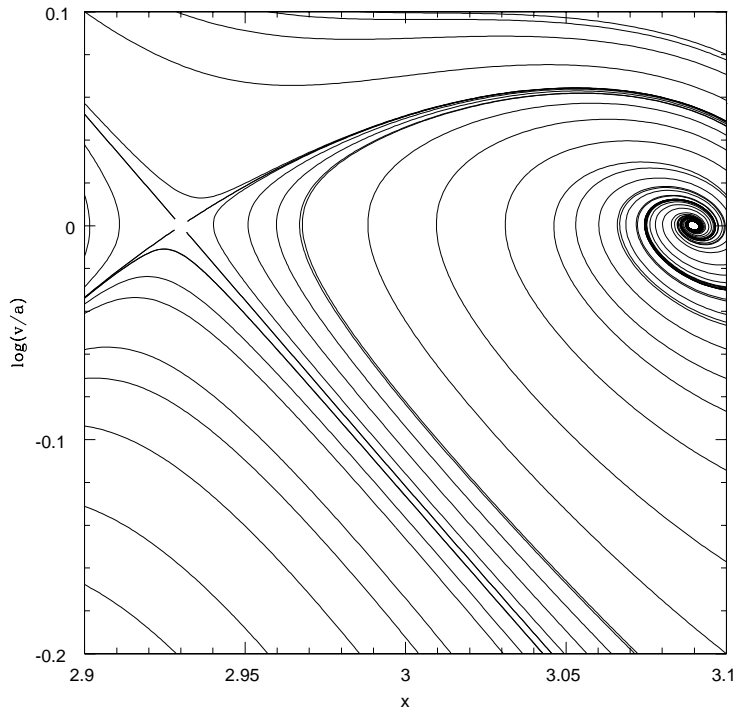


Fig. 8.— The vicinity of the critical points in the phase portrait of Fig. 7.

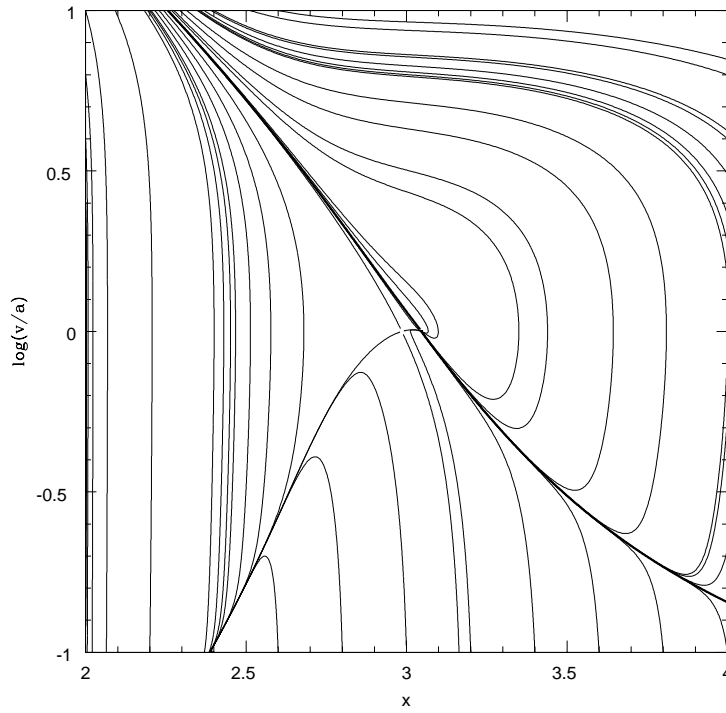


Fig. 9.— The Phase Portrait for  $a = 0.01$ ,  $\alpha = 0.1$  and  $x_c \simeq 3.047$ . The physical solution (thick curve) passes a critical point of the nodal type, in the fast direction.

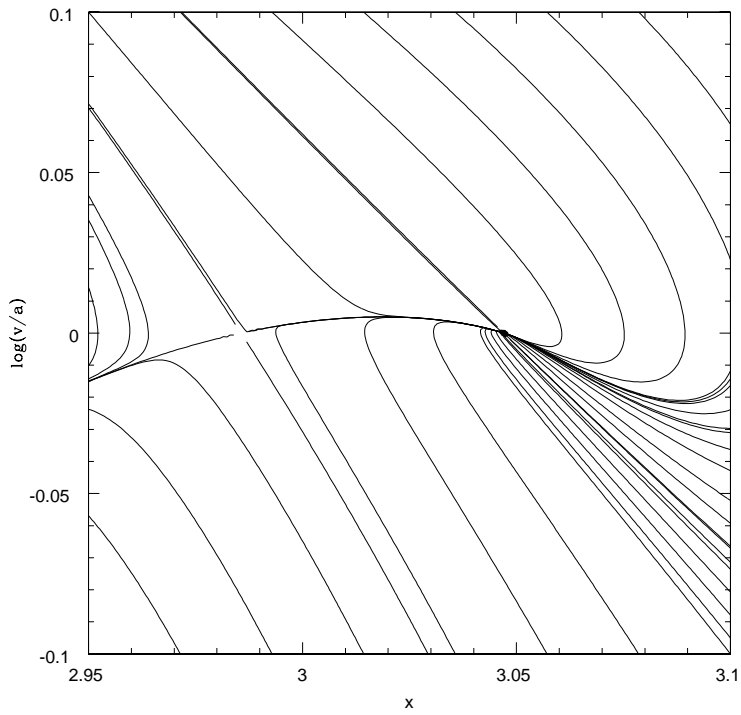


Fig. 10.— The vicinity of the critical points in the phase portrait of Fig.(9).

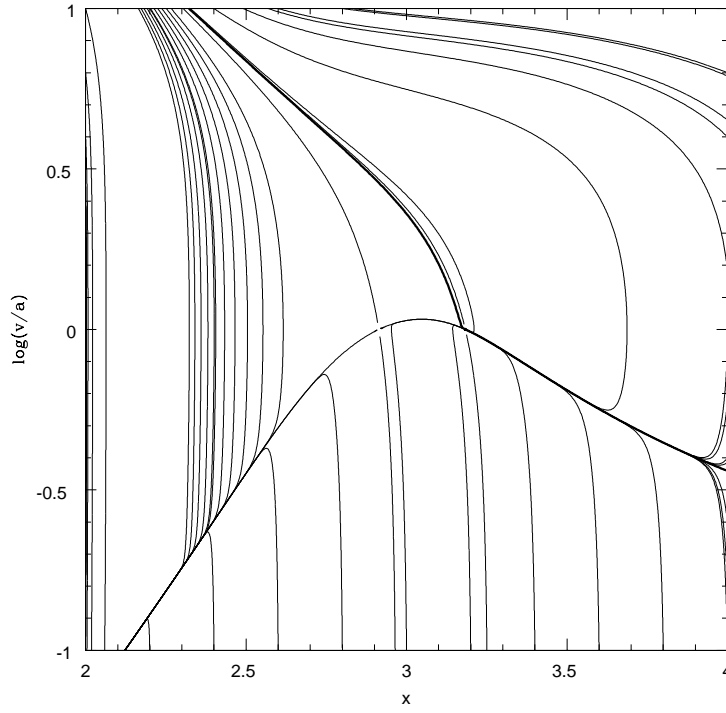


Fig. 11.— The Phase Portrait for  $a = 0.01, \alpha = 0.3$  and  $x_c \simeq 3.183$ . The physical solution (thick curve) passes a critical point of the nodal type, in the slow direction, analytically.

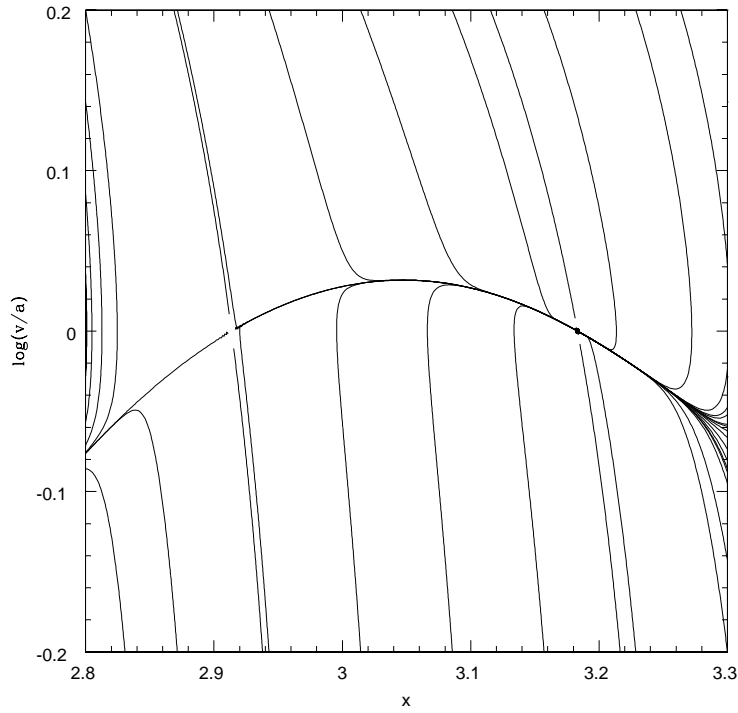


Fig. 12.— The vicinity of the critical points in the phase portrait of Fig.(11).